Photodoping-Modified Charge Density Wave Phase Transition in WS_2/1T-TaS_2 Heterostructure

Rui Wang(王瑞)[1,2†], Jianwei Ding(丁建伟)[2,4†], Fei Sun(孙飞)[5], Jimin Zhao(赵继民)[3,4,6*], and Xiaohui Qiu(裘晓辉)[2,4*]

[1]*Beijing Information Technology College, Beijing 100015, China*
[2]*CAS Key Laboratory of Standardization and Measurement for Nanotechnology, CAS Center for Excellence in Nanoscience, National Center for Nanoscience and Technology, Beijing 100190, China*
[3]*Beijing National Laboratory for Condensed Matter Physics, Institute of Physics, Chinese Academy of Sciences, Beijing 100190, China*
[4]*University of Chinese Academy of Sciences, Beijing 100049, China*
[5]*Max Planck Institute for Chemical Physics of Solids, Dresden 01187, Germany*
[6]*Songshan Lake Materials Laboratory, Dongguan 523808, China*

(Received 6 March 2024; accepted manuscript online 23 April 2024)

Controlling collective electronic states hold great promise for development of innovative devices. Here, we experimentally detect the modification of the charge density wave (CDW) phase transition within a 1T-TaS_2 layer in a WS_2/1T-TaS_2 heterostructure using time-resolved ultrafast spectroscopy. Laser-induced charge transfer doping strongly suppresses the commensurate CDW phase, which results in a significant decrease in both the phase transition temperature (T_c) and phase transition stiffness. We interpret the phenomenon that photo-induced hole doping, when surpassing a critical threshold value of $\sim 10^{18}\,\mathrm{cm}^{-3}$, sharply decreases the phase transition energy barrier. Our results provide new insights into controlling the CDW phase transition, paving the way for optical-controlled novel devices based on CDW materials.

DOI: 10.1088/0256-307X/41/5/057801

Metallic layered transition metal dichalcogenides exhibit a rich set of charge density wave (CDW) phases in which both the conduction electrons and the atomic structure display translational symmetry breaking.[1] Each phase transition is accompanied by a periodic distortion of the lattice, resulting in a strong modification of the electronic properties of the material.[2–7] The capability to control CDW states offers a way to deeply understand the CDW formation mechanisms and develop new functional devices. Modulation of the phase transition in thin-film 1T-TaS_2 by electric,[2] or light field[8,9] has been achieved experimentally, which has been used to construct oscillators operating at room temperature.[3,8] Due to the manifold effects induced by the external field, the tuning of the phase transition has been attributed to various effects, including the carrier doping effect,[10] Joule heating,[8,11,12] CDW depinning,[5] and strain.[13–16] A more quantitative assessment of these effects might be meaningful for both the fundamental physics and device applications.

Charge transfer doping in van der Waals (vdW) heterostructure (HS), accompanied by interfacial strain and band structure modulation,[17] has the potential to influence the electronic instabilities, thereby providing a novel platform for understanding and manipulating the CDW states. Recently, controlling CDW states by constructing vdW HS has been reported.[18–23] In the 1T-TaS_2/BP HS, a combination of interface effects, including orbital hybridization, strain, and charge transfer, leads to a suppressed and anisotropic commensurate CDW (CCDW) phase, resulting in gate-dependent conductance oscillations.[18] The interfacial electron transfer suppresses the CDW states by hindering the lattice distortion of 2H-$NbSe_2$ in graphene/$NbSe_2$ HS.[19]

Optical pump-probe spectroscopy is a unique tool for studying the formation of diverse CDW orders with temperature, which offers valuable insights into the nonequilibrium carrier dynamics of correlated materials.[24,25] In this work, we employ time-resolved spectroscopy to investigate the modification of the CDW phase transition in WS_2/1T-TaS_2 HS. By directly comparing the phase transition process between pristine 1T-TaS_2 and corresponding WS_2/1T-TaS_2 HS, we distinguish the distinctive roles of photo-induced charge transfer doping in influencing the CDW phase. Our results indicate that photo-induced doping is an efficient method to tune the CDW phases of the system, which is of pivotal importance for constructing devices based on CDW materials.

Our WS_2/1T-TaS_2 HS is fabricated using mechanical exfoliation and dry transfer method.[19,26] The 1T-TaS_2 thin films with different thicknesses are mechanically exfoliated on the SiO_2/Si substrate, followed by the characterization of the thickness using an atomic force micro-

†These authors contributed equally to this work.
*Corresponding authors. Email: jmzhao@iphy.ac.cn; xhqiu@nanoctr.cn
© 2024 Chinese Physical Society and IOP Publishing Ltd

scope. Subsequently, a monolayer WS_2 sample is obtained through mechanical exfoliation on a polydimethylsiloxane (PDMS) substrate and then transferred onto the 1T-TaS_2 thin films using the dry transfer method (see Fig. S1 in the Supplementary Materials). The sample thus prepared is annealed at 200 °C in an argon gas environment with a base pressure of 5 Torr for 4 h. All 1T-TaS_2 thin films with different thicknesses are partially covered by monolayer WS_2 (see Fig. S2). As depicted, the sample contains regions of monolayer WS_2, pristine 1T-TaS_2 films, and WS_2/1T-TaS_2 HS, thus facilitating their direct comparison. The Raman spectrum of the samples further confirms that the HS has been constructed successfully, the detailed discussion is given in the Supplementary Materials (SMs).

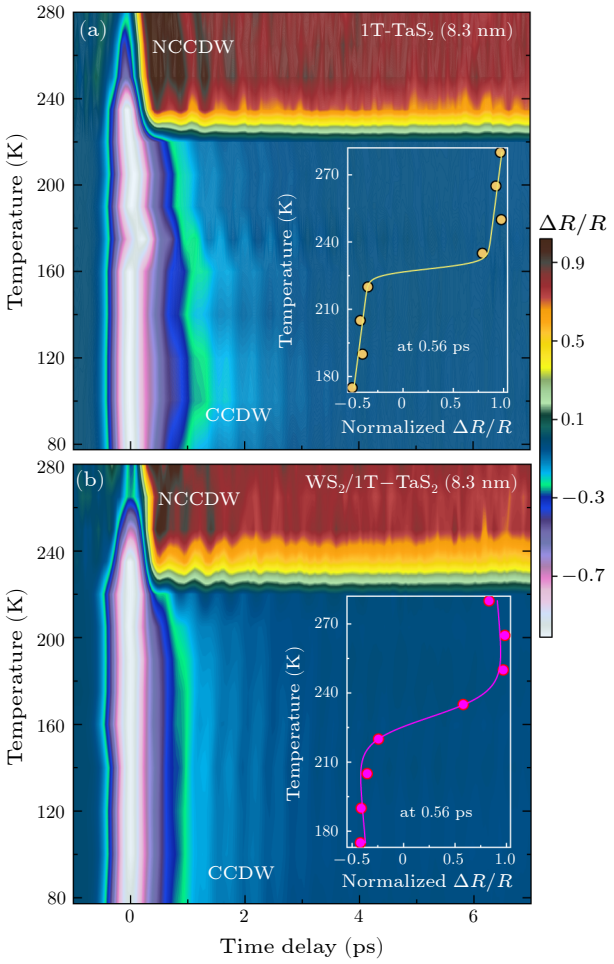

Fig. 1. Temperature-dependent normalized differential reflectivity $\Delta R/R$ for 1T-TaS_2 (8.3 nm) (a) and WS_2/1T-TaS_2 (8.3 nm) HS (b). The wavelengths of the pump and probe are 600 nm and 780 nm, respectively. The pump fluence is 9.7 μJ·cm^{-2}, and the probe fluence is 2.8 μJ·cm^{-2}. Insets: temperature-dependent normalized $\Delta R/R$ at 0.56 ps for 1T-TaS_2 (8.3 nm) (a) and WS_2/1T-TaS_2 (8.3 nm) HS (b). The solid lines in the insets are the guidelines, no physical meaning.

We investigate in depth the modulation of the CDW phase transition in WS_2/1T-TaS_2 (8.3 nm) HS using microscopic pump-probe spectroscopy. The laser system we used is based on a Ti:sapphire oscillator and an optical parametric oscillator (OPO) (76 MHz repetition rate, 100 fs pulse duration, Coherent, Inc.). The small partial output of the Ti:sapphire oscillator (780 nm) is employed as the probe beam, while the majority of 780 nm is used to excite the OPO, whose output is used as the pump beam. The detailed description of the pump-probe setup is given in the SMs, and the schematic of the optical pump-probe setup is also illustrated in Fig. S9. The pump pulse with a central wavelength of 600 nm (2.06 eV) and a fluence of 9.7 μJ·cm^{-2} excites electrons to the conduction band of WS_2, leading to the hole transferred to 1T-TaS_2 (see details in the SMs). The estimated photogenerated carrier density is $\sim 4 \times 10^{11}$ cm^{-2}, by using the absorption coefficient of 2×10^5 cm.[27] The fluence of the probe beam with the wavelength of 780 nm is 2.8 μJ·cm^{-2}. The thermal effect of the two beams is reasonably negligible due to the low fluences.[28]

The signal we detect (Fig. 1) is mainly coming from the 1T-TaS_2 layer, because the signal from the capping monolayer WS_2 has much smaller amplitude and very different relaxation process (Figs. S10 and S11). Thus, the temperature-dependent carrier dynamics of our HS can reveal the phase transition process of 1T-TaS_2 within the HS. Note that all the measurements are performed in a warming-up process. In Fig. 1, the temperature-dependent normalized differential reflectivity $\Delta R/R$ for 1T-TaS_2 (8.3 nm) and WS_2/1T-TaS_2 (8.3 nm) HS is presented. The phase transition features can be clearly identified [insets in Figs. 1(a) and 1(b)]. The phase transition process of 1T-TaS_2 (8.3 nm) appears to be faster compared to that observed in WS_2/1T-TaS_2 (8.3 nm) HS, which is further confirmed by the temperature-dependent dynamics that will be discussed in the following.

Previous ultrafast investigations have revealed different processes contributing to the photoinduced reflectivity transients in 1T-TaS_2: the exponential relaxations can be attributed to the single-particle relaxation across the CDW/Mott gap, while the oscillatory response is dominated by the coherently excited CDW amplitude mode (AM), but can also contain oscillatory components due to $q = 0$ optical phonons or zone folded-phonons.[7,28–30] Usually AMs are the most pronounced, as they can be effectively driven by optical excitation.[31] Summing up all the contributions, the photoinduced change in differential reflectivity $\Delta R/R$ can be expressed as[28,29,31,32]

$$\Delta R/R = A(T)e^{-t/\tau_{\rm AM}}\cos(\omega t + \varphi) + S(T)e^{-t/\tau_1} + P(T)e^{-t/\tau_2} + D(T), \quad (1)$$

where the first term on the right-hand side describes the AM of the CDW in 1T-TaS_2,[33] the second term corresponds to electron-phonon coupling, the third term is attributed to phonon-phonon scattering,[7] and the last term is a constant background, accounting for a bolometric response. The lifetime of the AM ($\tau_{\rm AM}$) can be determined by fitting the real-time oscillation, assuming a negligible contribution from the zone-folded peaks. Because the folded phonons are very weak for thin film samples, it is suitable to do so.[28] The relaxation is analyzed using two exponential fits [Eq. (1)].

Normalized $\Delta R/R$ for 1T-TaS_2 (8.3 nm) and WS_2/1T-TaS_2 (8.3 nm) at 77.4 K is plotted in Figs. 2(a) and 2(c). An oscillatory response is superimposed on the relaxation transient, which is consistent with the previous reports.[28,34] The oscillation [the insets in Figs. 2(a) and 2(c)] dominantly comprises of frequencies of 1.45 THz, 2.36/2.38 THz (AM) (Fig. S12).[34] The coexistence of a coherent phonon of 1.45 THz leads to difficulties in extracting the τ_{AM}, thus we track the phase transition process using the exponential decays.

According to Eq. (1), we obtain τ_1 and τ_2, as plotted in Figs. 2(b) and 2(d) for the 1T-TaS_2 (8.3 nm) and WS_2/1T-TaS_2 (8.3 nm) HS, respectively. For 1T-TaS_2 (8.3 nm), τ_1 rapidly drops from $\sim$0.4 ps to $\sim$ 0.18 ps owing to the CCDW-NCCDW transition, indicating that the phase transition stiffness (PTS) is in the range from 220 K to 235 K. It is necessary to point out that the PTS describes how the phase transition is immune to the external factors, rather than how stiff the phase itself is. The sharper the phase transition is, the larger the PTS is.[28] In parallel, τ_2 decreases with increasing temperature and immediately vanishes when the discommensuration network appears. For WS_2/1T-TaS_2 (8.3 nm) HS, the temperature-dependent τ_1 implies that the PTS is between 205 K and 250 K, suggesting that the phase transition process of 1T-TaS_2 is significantly modulated within HS. It is important to note that the change in the PTS of HS is not attributed to the variation in thickness, since the thickness of 1T-TaS_2 in HS is the same as that of the pristine 1T-TaS_2. Additionally, the phase transition process can also be identified from the temperature dependence of the $\Delta R/R$ amplitude,[35] as illustrated in Fig. S13.

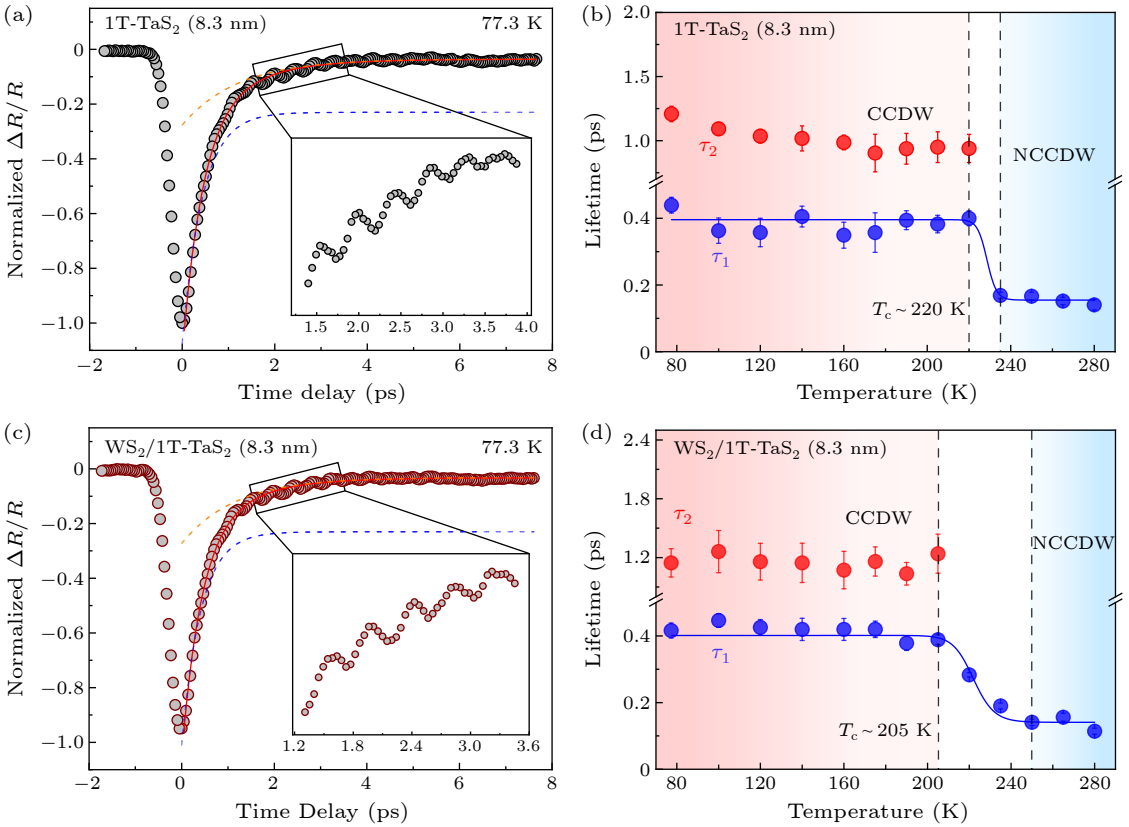

Fig. 2. Typical normalized differential reflection $\Delta R/R$ at the temperature of 77.4 K for 1T-TaS_2 (8.3 nm) (a) and WS_2/1T-TaS_2 (8.3 nm) HS (c). The wavelengths of pump and probe pulse are 600 nm and 780 nm, respectively. The pump fluence is 9.7 $\mu J \cdot cm^{-2}$, and the probe fluence is 2.8 $\mu J \cdot cm^{-2}$. The insets of (a) and (c) are the expanded views of (a) and (c) within a short time range, respectively. The red curves in (a) and wine solid curves in (c) are the fitting curves using two-exponential function. Dashed curves: two composing components (blue: electron-phonon coupling; orange: phonon-phonon scattering). Temperature-dependent τ_1 and τ_2 for 1T-TaS_2 (8.3 nm) (b) and WS_2/1T-TaS_2 (8.3 nm) HS (d) are plotted. The phase transition starts at 220 K and ends at $\sim$235 K for 1T-TaS_2 (8.3 nm) as displayed in (b). The phase transition is from 205 K to $\sim$250 K for WS_2/1T-TaS_2 (8.3 nm) HS as shown in (d). Both the dotted lines and the blue solid lines in (b) and (d), are the guidelines.

Next, we focus on the photoinduced interfacial charge transfer. We use a new pump beam with a longer wavelength (650 nm), while keeping the rest of the experimental parameters identical to the aforementioned ones in Figs. 1 and 2. In this case, the photo energy of the 650 nm laser (1.9 eV) is smaller than the band gap of WS_2 ($\sim$2.01 eV), which is not able to excite electrons to its conduction band, i.e., no photoinduced charge transfer. The results are shown in Fig. S14. The oscillatory response superimposed in $\Delta R/R$ exhibits the frequencies: 1.45 THz, and

2.42/2.41 THz (AM). The τ_1 and τ_2 can be obtained by using Eq. (1), as plotted in Figs. S14(c) and S14(d) for the 1T-TaS_2 (8.3 nm) and WS_2/1T-TaS_2 (8.3 nm) HS, respectively. The phase transition occurs between 220 K and 235 K for 1T-TaS_2 (8.3 nm), while the PTS range is from 205 K to 250 K for WS_2/1T-TaS_2 (8.3 nm) HS. Notably, these results are similar to the features observed under the 600 nm laser excitation, demonstrating that photoinduced doping has no detectable effect on the CDW transition in this case. Here, the primary factor contributing to the suppression of T_c by 15 K ($\Delta T_{\text{no-doping}} = 15$ K) and the reduction of the PTS may come from the interface itself (see the SMs).

Under the pump fluence of 9.7 $\mu J \cdot cm^{-2}$ with the 600 nm excitation, the estimated photo-excited carrier density in WS_2 is $\sim 4 \times 10^{11}$ cm^{-2}, as mentioned above. The charge transfer efficiency in the WS_2/1T-TaS_2 (8.3 nm) heterostructure is assumed to be 97%, as indicated by the quenching of its photoluminescence intensity to 3% of monolayer WS_2 (Fig. S8). Note that this assumption is based on the weakly temperature-dependent charge transfer efficiency in van der Waals heterostructures[36] and may potentially overestimate the charge transfer efficiency. The photoinduced hole doping density is 5×10^{17} cm^{-3}, assuming a uniform distribution in 1T-TaS_2. Such a photoinduced hole doping density is two orders of magnitude smaller than the critical carrier density of CCDW-NCCDW transition ($\sim 5 \times 10^{19}$ cm^{-3}).[5,37] Therefore, there is unlikely photodoping-modified CDW transition.

To gain insights into the photodoping-modulated phase transition, we performed the phase transition as a function of hole doping density. The hole doping density is expressed as $n_{\text{photodoping}} = \frac{\int \frac{F}{h\nu e^{-\alpha z}} dz \times \eta}{d}$ (here it is assumed that the transferred holes are uniformly distributed throughout the 1T-TaS_2), where F is the pump fluence, η represents the transfer efficiency which can be obtained by the PL quenching, α is the absorption coefficient of WS_2, and d is the thickness of 1T-TaS_2 within HS. The high doping density can be achieved by either increasing the pump fluence (such as 9.7, 19.5, 29.2 $\mu J \cdot cm^{-2}$) or reducing the thickness of 1T-TaS_2 (see details in the SMs).

For HS with very thin 1T-TaS_2, the amplitude of ΔR is comparable to that of pristine WS_2 (Fig. S10), making it too subtle to extract the T_c from the exponential decays. The transition temperature can be extracted from the temperature-dependent τ_{AM}, as it has been verified for thin pristine 1T-TaS_2 in our previous work.[28] In Fig. 3, the T_c and PTS for 1T-TaS_2 (4.4 nm) and WS_2/1T-TaS_2 (4.4 nm) HS are determined based on the temperature-dependent behavior of τ_{AM}. T_c exhibits a decrease with increasing photodoping density, while the completion temperature of the phase transition shows weak dependence on doping density. Consequently, as presented in Table S2, the range of the PTS expands with higher doping density, i.e., the PTS decreases with increasing doping density. This observation could be attributed to the hole doping inhibiting the nucleation and growth of discommensurations. Note that T_c of the 4.4 nm pristine 1T-TaS_2 is nearly independent of the pump fluence (Fig. S18), and that for the 9.2 nm pristine 1T-TaS_2 is also independent of the pump fluence (Fig. S15). These observations demonstrate that the reduction of T_c in Fig. 3 is not due to laser heating.

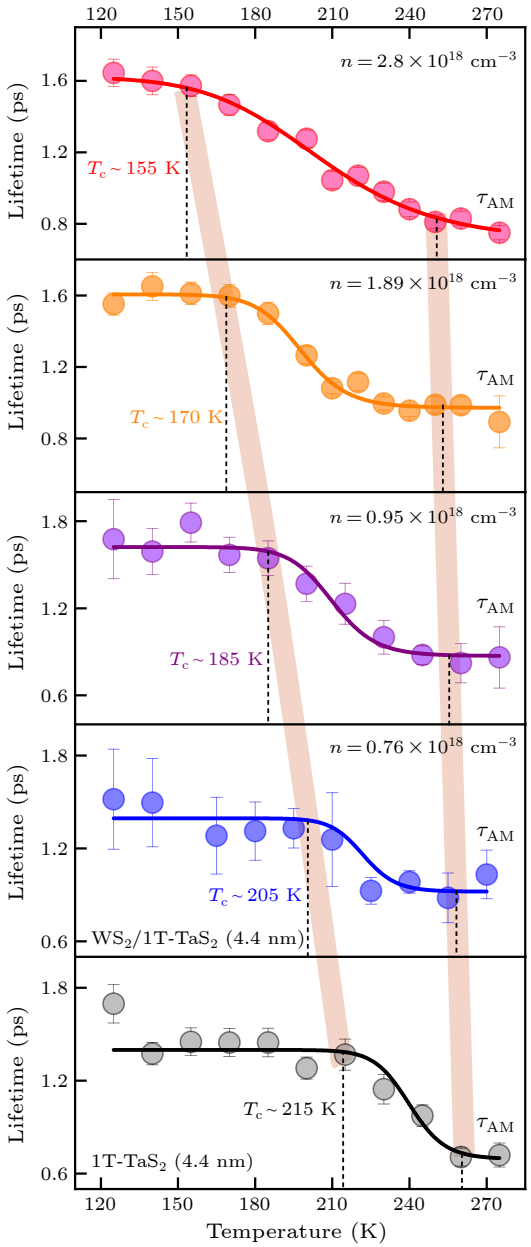

Fig. 3. Temperature dependent lifetime of AM (τ_{AM}) for WS_2/1T-TaS_2 (4.4 nm) HS under different photo-induced hole doping, and that of 1T-TaS_2 (4.4 nm) as a reference. Both the T_c and PTS decrease with increasing hole doping density. Here, the PTS describes how the phase transition is immune to the external factors, rather than how stiff the phase itself is. The sharper the phase transition is, the larger the PTS is. The wavelengths of pump and probe pulse are 600 nm and 780 nm, respectively. Both the dotted lines and the solid lines are the guidelines with no physical meaning.

To isolate the impact of charge transfer doping, we subtract the effects originating from interface itself in the following discussion. For WS_2/1T-TaS_2 (8.3 nm) HS, $\Delta T_{\text{no-doping}}$ is 15 K. Similarly, for WS_2/1T-TaS_2 (5.1 nm)

HS, $\Delta T_{\text{no-doping}}$ is also 15 K, as illustrated in Fig. S17. Therefore, it is inferred that the $\Delta T_{\text{no-doping}}$ is 15 K for HS samples (the thickness of 1T-TaS_2 is $\lesssim$8.3 nm) in our study.

Figure 4(a) presents a schematic diagram of the photoinduced hole-doping mechanism. Electron–hole pairs are initially light-induced in the monolayer WS_2. Then, the holes quickly transfer to the 1T-TaS_2 layer, while electrons remain in the WS_2 layer. The hole doping-induced ΔT_{doping} ($\Delta T_{\text{doping}} = T_c|_{1T\text{-}TaS_2} - T_c|_{\text{HS}} - \Delta T_{\text{no-doping}}$) is plotted in Fig. 4(b). For doping density $\lesssim 0.8\times10^{18}$ cm^{-3}, the CDW phase remains relatively robust, while once the doping density is $\gtrsim 1\times10^{18}$ cm^{-3}, the phase transition becomes sensitive to the doping level, which can be significantly modulated. The threshold-like behavior in the phase transition of pristine 1T-TaS_2, triggered by gate voltage,[3,38] has been reported, providing further corroboration and validation for our findings. In addition, note that the uncertainty of ΔT_{doping} determined from the experiments [i.e., the magnitude of error bar in Fig. 4(b)] depends on the temperature interval of the experiments, which means that, even when the doping density is smaller than 1×10^{18} cm^{-3}, a ΔT_{doping} less than 10 K is still achievable. The low doping level regime would be interesting in the case of finer tuning of the transition. However, one needs to be more careful of the other effects such as laser heating when probing within that regime.

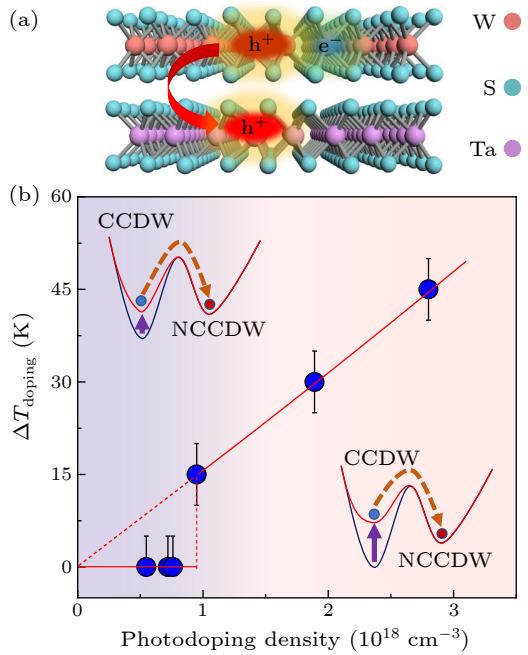

Fig. 4. Schematic illustration of charge transfer between the WS_2 and 1T-TaS_2 layers (a). Photodoping-modified phase transition (b). Here, $\Delta T_{\text{doping}} = T_c|_{1T\text{-}TaS_2} - T_c|_{\text{HS}} - \Delta T_{\text{no-doping}}$. The inset in (b) shows how the photo-induced hole doping affects the CDW phase transition.[10] Red curve: a guide to the eyes.

In pristine 1T-TaS_2, the CCDW phase has a lower energy, so the system needs to overcome a higher energy barrier to transform into the NCCDW phase. Hole-doping into a David star cluster reduces the charge density at the center and the inner atoms, weakening the charge density clustering. Simultaneously, the electron-phonon coupling at the CDW vector is reduced by the hole doping.[10] Consequently, holes lead to an increase in the energy of the CCDW phase, effectively lowering the energy barrier associated with the phase transition [inset of Fig. 4(b)]. It has been demonstrated that this energy barrier decreases linearly with increasing doping density.[39] In the low doping regime, the energy barrier undergoes a weak reduction, exerting minimal influence on the phase transition process and resulting in a relatively robust T_c [upper inset in Fig. 4(b)]. Conversely, at high doping levels, the energy barrier experiences a pronounced reduction, leading to easier phase transition [lower inset in Fig. 4(b)]. The higher the doping density, the lower the energy barrier, facilitating an easier transition from CDDW to NCCDW. As shown in Fig. 4(b), ΔT_{doping} is proportional to the hole-doping density. The red line is a fitting line, whose extension passes through the (0, 0) point of the coordinate. This further indicates that laser-induced hole doping is the factor controlling the CDW phase transition.

A semi-quantitative comparison is the laser-induced doping density concerning the intrinsic carrier density. According to the previous Hall effect investigation,[37] the carrier density at 155 K under the CCDW phase is $\sim8\times10^{18}$ cm^{-3}. Our results indicate that with optical doping at about 37% of the intrinsic carrier density (i.e., $\sim3\times10^{18}$ cm^{-3}), the system can initiate a phase transition. This strongly indicates that photo-induced doping is an efficient method to tune the CDW phases of the system, providing a guideline for the optical tuning efficiency in future studies.

In summary, we have investigated the modulation of the phase transition of 1T-TaS_2 within WS_2/1T-TaS_2 HS using microscopic time-resolved ultrafast spectroscopy. Our findings reveal a significant suppression of the CCDW state owing to photoinduced-hole doping. Both the T_c and PTS decrease with increasing light-induced hole doping density. This effect becomes more pronounced when the hole doping density is above a threshold-like value of $\sim10^{18}$ cm^{-3}. Photo-induced doping density removes the phase transition energy barrier, which facilitates a more accessible phase transition. Our results provide profound insights into the manipulation of the CDW states, offering valuable perspectives for development of novel devices based on correlated materials.

Acknowledgments. This work was supported by the National Key Research and Development Program of China (Grant No. 2021YFA1400201), the CAS Project for Young Scientists in Basic Research (Grant No. YSBR-059), the Beijing Natural Science Foundation (Grant No. 4191003), the National Natural Science Foundation of China (Grant No. 11774408), the Scientific Instrument Developing Project of the Chinese Academy of Sciences (Grant No. GJJSTD20200005), the Strategic Priority Research Program of Chinese Academy of Sciences (Grant Nos. XDB36000000 and XDB30000000), the International Partnership Program of Chinese Academy of Sciences (Grant No. GJHZ1826), and CAS Interdisciplinary Innovation Team.

References

[1] Tsen A W, Hovden R, Wang D *et al.* 2015 *Proc. Natl. Acad. Sci. USA* **112** 15054

[2] Yoshida M, Suzuki R, Zhang Y, Nakano M, and Iwasa Y 2015 *Sci. Adv.* **1** e1500606

[3] Liu G, Debnath B, Pope T R, Salguero T T, Lake R K, and Balandin A A 2016 *Nat. Nanotechnol.* **11** 845

[4] Yu Y J, Yang F Y, Lu X F *et al.* 2015 *Nat. Nanotechnol.* **10** 270

[5] Hollander M J, Liu Y, Lu W J, Li L J, Sun Y P, Robinson J A, and Datta S 2015 *Nano Lett.* **15** 1861

[6] Wen W, Zhu Y, Dang C, Chen W, and Xie L 2019 *Nano Lett.* **19** 1805

[7] Hasaien J Z L, Wu Y L, Shi M Z, Zhai Y N, Wu Q, Liu Z, Zhou Y, Chen X H, and Zhao J M 2024 submitted

[8] Zhu C, Chen Y, Liu F C *et al.* 2018 *ACS Nano* **12** 11203

[9] Li W and Naik G V 2020 *Nano Lett.* **20** 7868

[10] Shao D F, Xiao R C, Lu W J, Lv H Y, Li J Y, Zhu X B, and Sun Y P 2016 *Phys. Rev. B* **94** 125126

[11] Mohammadzadeh A, Baraghani S, Yin S, Kargar F, Bird J P, and Balandin A A 2021 *Appl. Phys. Lett.* **118** 093102

[12] Jarach Y, Rodes L, Ber E, Yalon E, and Kanigel A 2022 *Appl. Phys. Lett.* **120** 083502

[13] Svetin D, Vaskivskyi I, Sutar P, Goreshnik E, Gospodaric J, Mertelj T, and Mihailovic D 2014 *Appl. Phys. Express* **7** 103201

[14] Gan L Y, Zhang L H, Zhang Q Y, Guo C S, Schwingenschlögl U, and Zhao Y 2016 *Phys. Chem. Chem. Phys.* **18** 3080

[15] Zhao R, Wang Y, Deng D, Luo X, Lu W J, Sun Y P, Liu Z K, Chen L Q, and Robinson J 2017 *Nano Lett.* **17** 3471

[16] Bu K, Zhang W, Fei Y, Wu Z, Zheng Y, Gao J, Luo X, Sun Y P, and Yin Y 2019 *Commun. Phys.* **2** 146

[17] Manzeli S, Ovchinnikov D, Pasquier D, Yazyev O V, and Kis A 2017 *Nat. Rev. Mater.* **2** 17033

[18] Wang Z, Chu L, Li L, Yang M, Wang J, Eda G, and Loh K P 2019 *Nano Lett.* **19** 2840

[19] Chen Y, Wu L S, Xu H *et al.* 2020 *Adv. Mater.* **32** 2003746

[20] Fu W, Qiao J S, Zhao X X *et al.* 2020 *ACS Nano* **14** 3917

[21] Zhao W M, Zhu L, Nie Z, Li Q Y, Wang Q W, Dou L G, Hu J G, Xian L, Meng S, and Li S C 2022 *Nat. Mater.* **21** 284

[22] Szałowski K, Milivojević M, Kochan D, and Gmitra M 2023 *2D Mater.* **10** 025013

[23] Lutsyk I, Szalowski K, Krukowski P *et al.* 2023 *Nano Res.* **16** 11528

[24] Wu Q, Zhou H X, Wu Y L, Hu L L, Ni S L, Tian Y C, Sun F, Zhou F, Dong X L, Zhao Z X, and Zhao J M 2020 *Chin. Phys. Lett.* **37** 097802

[25] Hao W J, Gu M H, Tian Z Y, Fu S H, Meng M, Zhang H, Guo J D, and Zhao J M 2024 *Adv. Sci.* **11** 2305900

[26] Wang K, Huang B, Tian M K *et al.* 2016 *ACS Nano* **10** 6612

[27] Liu H L, Shen C C, Su S H, Hsu C L, Li M Y, and Li L J 2014 *Appl. Phys. Lett.* **105** 201905

[28] Wang R, Zhou J B, Wang X S, Xie L M, Zhao J M, and Qiu X H 2021 *Nano Res.* **14** 1162

[29] Demsar J, Biljaković K, and Mihailovic D 1999 *Phys. Rev. Lett.* **83** 800

[30] Warawa K, Christophel N, Sobolev S, Demsar J, Roskos H G, and Thomson M D 2023 *Phys. Rev. B* **108** 045147

[31] Toda Y, Tateishi K, and Tanda S 2004 *Phys. Rev. B* **70** 033106

[32] Yusupov R V, Mertelj T, Chu J H, Fisher I R, and Mihailovic D 2008 *Phys. Rev. Lett.* **101** 246402

[33] Demsar J, Forró L, Berger H, and Mihailovic D 2002 *Phys. Rev. B* **66** 041101

[34] Dardel B, Grioni M, Malterre D, Weibel P, Baer Y, and Lévy F 1992 *Phys. Rev. B* **46** 7407

[35] Kabanov V V, Demsar J, Podobnik B, and Mihailovic D 1999 *Phys. Rev. B* **59** 1497

[36] Kozawa D, Carvalho A, Verzhbitskiy I, Giustiniano F, Miyauchi Y, Mouri S, Neto A H C, Matsuda K, and Eda G 2016 *Nano Lett.* **16** 4087

[37] Inada R, Ōnuki Y, and Tanuma S 1979 *Phys. Lett.* **69** 453

[38] Yoshida M, Zhang Y, Ye J, Suzuki R, Imai Y, Kimura S, Fujiwara A, and Iwasa Y 2014 *Sci. Rep.* **4** 7302

[39] Dang C, Guan M, Hussain S, Wen W, Zhu Y, Jiao L, Meng S, and Xie L 2020 *Nano Lett.* **20** 6725